

Tough-interface-enabled stretchable electronics using non-stretchable polymer semiconductors and conductors

Received: 17 February 2022

Accepted: 4 September 2022

Published online: 10 November 2022

 Check for updates

Jiheong Kang^{1,2,5}, Jaewan Mun^{1,5}, Yu Zheng¹, Masato Koizumi³, Naoji Matsuhisa¹, Hung-Chin Wu¹, Shucheng Chen¹, Jeffrey B.-H. Tok¹, Gae Hwang Lee⁴, Lihua Jin¹✉ & Zhenan Bao¹✉

Semiconducting polymer thin films are essential elements of soft electronics for both wearable and biomedical applications^{1–11}. However, high-mobility semiconducting polymers are usually brittle and can be easily fractured under small strains (<10%)^{12–14}. Recently, the improved intrinsic mechanical properties of semiconducting polymer films have been reported through molecular design^{15–18} and nanoconfinement¹⁹. Here we show that engineering the interfacial properties between a semiconducting thin film and a substrate can notably delay microcrack formation in the film. We present a universal design strategy that involves covalently bonding a dissipative interfacial polymer layer, consisting of dynamic non-covalent crosslinks, between a semiconducting thin film and a substrate. This enables high interfacial toughness between the layers, suppression of delamination and delocalization of strain. As a result, crack initiation and propagation are notably delayed to much higher strains. Specifically, the crack-onset strain of a high-mobility semiconducting polymer thin film improved from 30% to 110% strain without any noticeable microcracks. Despite the presence of a large mismatch in strain between the plastic semiconducting thin film and elastic substrate after unloading, the tough interface layer helped maintain bonding and exceptional cyclic durability and robustness. Furthermore, we found that our interfacial layer reduces the mismatch of thermal expansion coefficients between the different layers. This approach can improve the crack-onset strain of various semiconducting polymers, conducting polymers and even metal thin films.

Freestanding plastic thin films, such as polymers and metals, rupture primarily due to strain localization onto film defects²⁰. However, when such a thin film is supported on a polymer substrate, strain localization may be mitigated by the substrate; therefore, the thin film becomes

more tolerant to elongation and deformation. For example, a thin copper film (100 nm) on a polyimide substrate could sustain >50% strain, whereas a freestanding copper thin film breaks below 2% strain^{21,22}. Recently, crack suppression in a copper thin film (100 nm) was reported

¹Department of Chemical Engineering, Stanford University, Stanford, CA, USA. ²Department of Materials Science and Engineering, Korea Advanced Institute of Science and Technology (KAIST), Daejeon, Republic of Korea. ³Department of Mechanical and Aerospace Engineering, University of California, Los Angeles, CA, USA. ⁴Samsung Advanced Institute of Technology Yeongtong-gu, Suwon-si, South Korea. ⁵These authors contributed equally: Jiheong Kang, Jaewan Mun. ✉e-mail: lihuajin@seas.ucla.edu; zbao@stanford.edu

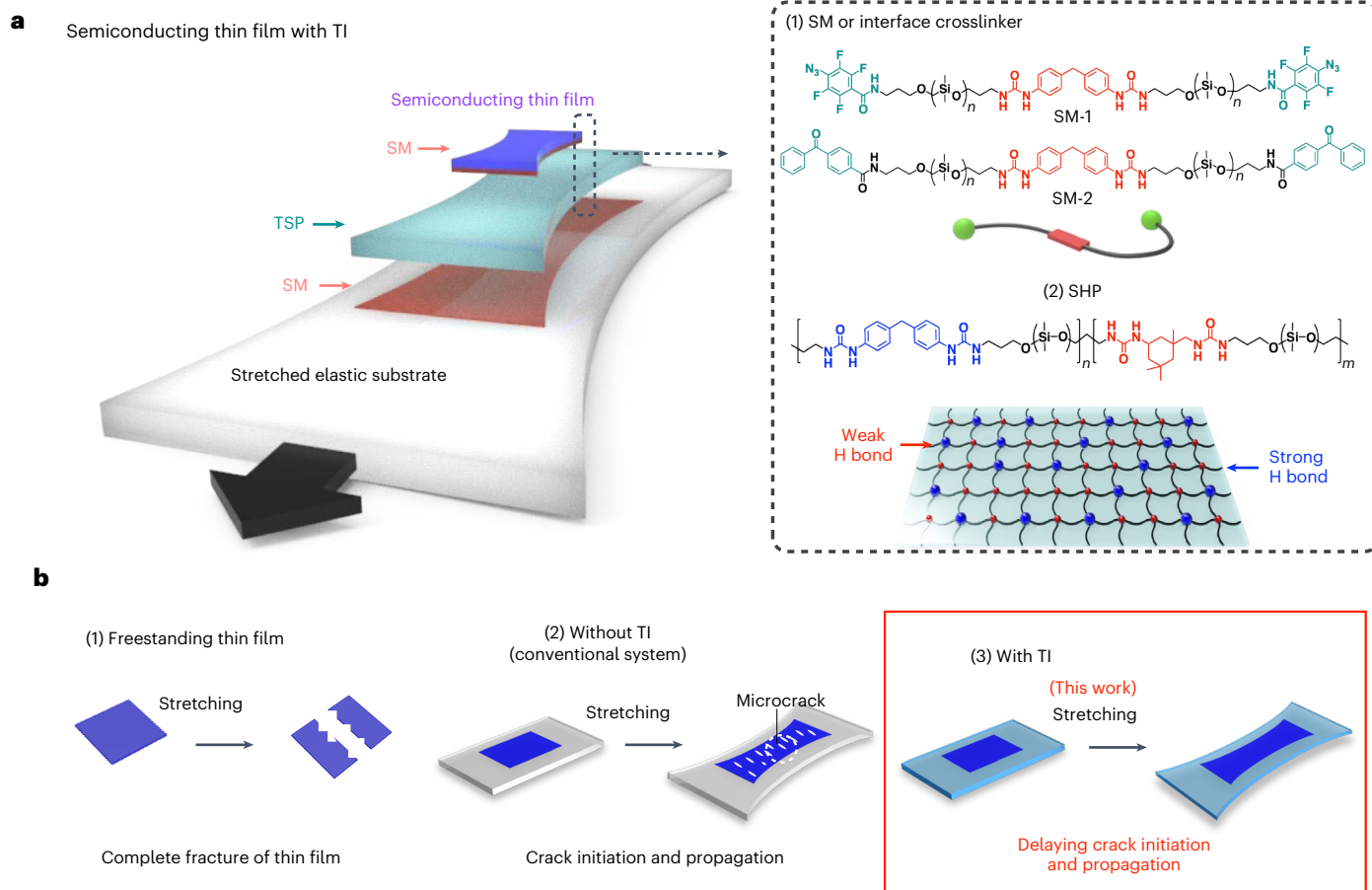


Fig. 1 | Introducing a TI between a semiconducting film and an elastic substrate. **a**, Schematic of a TI between a semiconducting film and an elastic substrate. The TI bonding is enabled by two essential chemical components: (1) SM and (2) siloxane-based SHP capable of self-recoverable energy dissipation. A TSP is composed of a mixture of 90 wt% SHP as the energy-dissipating matrix and 10 wt% SM as the crosslinker. **b**, Schematic of the fracture conditions of a

polymer thin film under various conditions. Under the freestanding condition (1), a polymer thin film undergoes brittle fracture separated into two pieces by stretching. When the thin film is attached onto an elastic polymer substrate (2), microcracks form in the polymer thin film instead of complete fracture. This work shows that embedding a TI layer delays crack initiation and propagation (3).

by improving the film adhesion on the substrate using electron-beam irradiation²³. Furthermore, design strategies for tough interfaces (TIs) between hydrogels and various solids have also been reported^{24–27}. One main concept is to introduce energy dissipation mechanisms into hydrogels, in conjunction with forming covalent bonding between the two materials. As a result, the interfacial toughness was notably increased^{25,26}. However, such TI strategies have not been applied to stretchable polymer electronics.

Here we present a TI design to impart stretchability to brittle semiconducting polymer thin films (Fig. 1a). Briefly, our TI bonding is enabled by two essential chemical components: (1) a tough self-healing polymer matrix (TSP) capable of repeated energy dissipation through autonomous dynamic bond breakage and reformation and (2) a surface modifier (SM) that both covalently and non-covalently bonds with the TSP and covalently bonds with the substrate (Fig. 1a). This enables TI bonding, prevents delamination, delocalizes strain in the film and finally notably delays crack propagation (Fig. 1b). A TSP is composed of a mixture of 90 wt% self-healing polymer (SHP) as the energy-dissipating matrix and 10 wt% SM as the crosslinker. Specifically, the SHP is a polydimethylsiloxane-based tough elastomeric network consisting of two kinds of hydrogen bonds (H bonds) with different bond strengths. The SM has the following three features: (1) two perfluorophenylazide or benzophenone moieties at the ends of a flexible chain for covalent bonding with any polymer surface by light

or heat²⁸, (2) a dynamic H-bonding unit for non-covalent interactions with TSP and (3) a flexible long polydimethylsiloxane chain ($M_w \approx 5,000$) for the stretchability of SM layer (Fig. 1a).

Figure 2a illustrates the preparation processes of the TI layer. Briefly, we first spin or dip coat a solution of SM (5 wt% in isopropanol (IPA)) on a polymer surface and covalently immobilize SM (7–8 nm) by ultraviolet irradiation for 10 min and thermal annealing at 150 °C for 10 min. The covalent surface modification was confirmed by X-ray photoelectron spectroscopy, Fourier-transform infrared spectroscopy and contact angle measurements (Supplementary Figs. 1–3). A TSP film (2 μm) composed of a mixture of 90 wt% SHP (the structure is shown in Fig. 1a) as the energy-dissipating matrix and 10 wt% SM as the crosslinker was laminated onto the SM-modified substrate. Subsequently, the resulting bilayer film was gradually heated to 150 °C over 15 min and annealed for 30 min to ensure covalent crosslinking. The adhesion energy between the two layers was measured by the 180° peeling test (Fig. 2a,b)²⁸. The measured values of interfacial fracture energy between TSP and various types of polymer substrate are well over 1,500 J m^{−2}, which is much higher than other reported dry adhesives²⁹ (Fig. 2a,c), indicating tough adhesion between the TSP and substrate.

To further understand the mechanisms for the achieved high interfacial fracture energy, we performed a number of control experiments. First, we observed that without the initial surface modification by SM, the interfacial fracture energy was only 6 J m^{−2} (Supplementary Fig. 4),

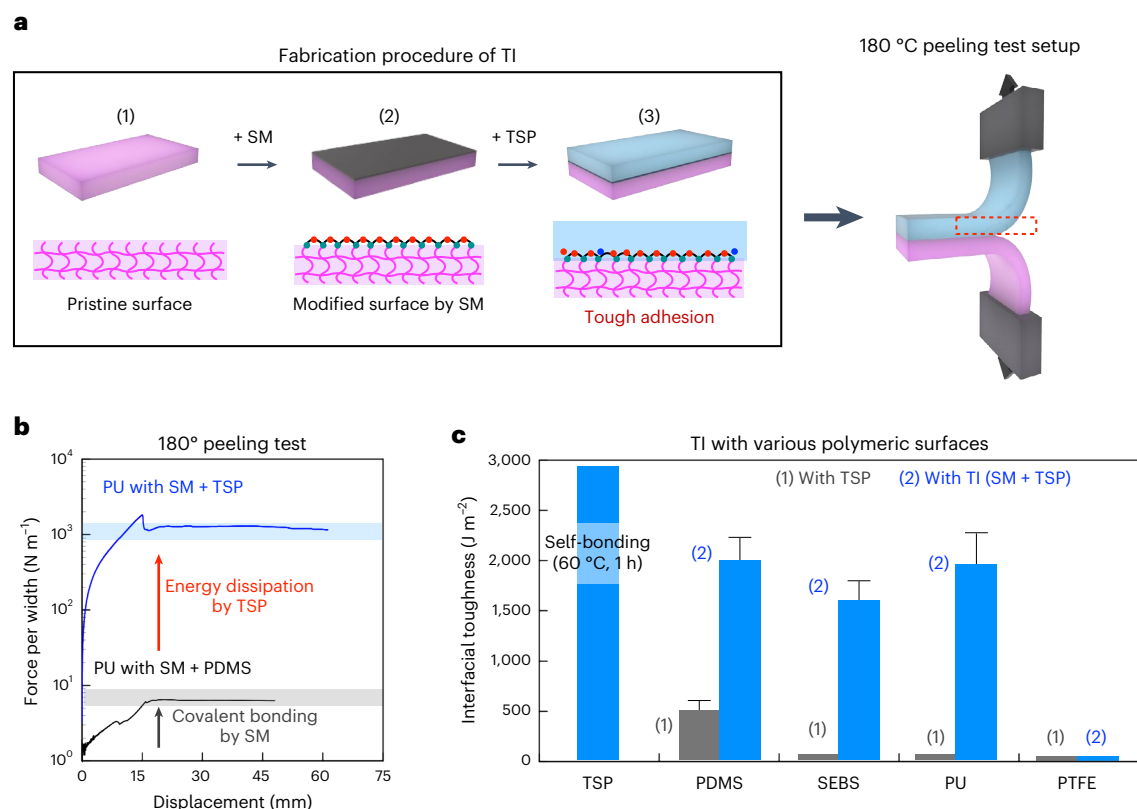


Fig. 2 | Fabrication and characterization of TI between TSP and various polymer substrates. **a**, Schematic of the fabrication procedure for the TI. An elastomer substrate (200 μm , 1) was surface modified by SM (7 nm, 2). Then, the TSP film (200 μm , 90 wt% SHP + 10 wt% SM, 3) was laminated and annealed at 150°C for 1 h. **b**, The measured peeling forces per width of the substrate as functions of the applied displacement for different types of interface (strain rate, 200% min^{-1}). The black arrow indicates the effect of a covalently

crosslinked interface. The red arrow indicates the effect of energy dissipation. **c**, Summary of the measured interfacial toughness of various elastomer/TI and elastomer/TSP. SEBS, styrene-ethylene-butylene-styrene thermoplastic elastomer; PU, polyurethane thermoplastic elastomer. SM could not be covalently fixed onto polytetrafluoroethylene (PTFE) due to the lack of CH_2 groups, resulting in poor adhesion. The error bars describe the standard error for three samples in each case.

suggesting that a thin SM layer is essential. Second, the H-bonding moieties in the SM structure were observed to be crucial. Without the H bonds, we observed relatively weak adhesion between TSP and other polymers (Supplementary Fig. 4). Third, when TSP was replaced with covalently crosslinked polydimethylsiloxane (PDMS; SYLGARD 184) instead of the SHP, the adhesion energy again was low due to the lack of energy dissipation mechanisms (Fig. 2c). We have previously shown the extremely high stretchability and fracture energy of this SHP, where a mixture of strong and weak H bonds together with highly flexible PDMS chains has been shown to effectively dissipate mechanical energy³⁰ (Supplementary Fig. 5). Therefore, the surface covalent bonding of SM combined with bulk dynamic H bonding for the energy dissipation of TSP resulted in high interfacial toughness. Previous work reported methods to realize high interface toughness with tough hydrogels^{24,25,27}. This work provides the molecular design for high interface toughness between various non-hydrogel materials. In addition, we confirmed that our TI ($1,300 \text{ J m}^{-2}$) can additionally be realized by benzophenone covalent crosslinkers and energy-dissipative polymer matrixes (Supplementary Fig. 4).

To demonstrate the utility of TI for improving the stretchability of brittle polymer thin films, we applied it first to a well-known high-mobility brittle semiconducting polymer (P1) thin film (40 nm; Fig. 1a). Various multilayer structures were fabricated, with the dimensions shown in Supplementary Fig. 6. Although embedding an interfacial layer between a film and substrate can function as a buffer layer to hinder fracture, predicted by a shear-lag model³¹, we show that this buffering effect is negligible in our multilayer structures, given their geometry and material properties (Methods). To more accurately

determine the strain in the semiconducting P1 film, we directly measured it using optical microscopy and used it to quantify the crack-onset strain of the film. To determine whether a TI between P1 and SM/TSP was indeed achieved, a simple ‘Scotch tape test’ was performed, in which a negligible delamination of the semiconducting layer from SM/TSP (TI) (Supplementary Fig. 7) was observed. Note that the 180° peeling test could not be performed because the semiconducting film typically used for devices are too thin ($<60 \text{ nm}$). In contrast, the transferred P1 on the PDMS substrate, which is typically used for the stretchability tests of semiconducting layers, was easily delaminated by the Scotch tape (Supplementary Fig. 7).

A pseudo-freestanding polymer thin film ($<100 \text{ nm}$) (for example, a film on water) typically ruptures at a smaller strain than its bulk films ($>100 \mu\text{m}$), which is attributed to strain localization in the bulk film²⁰. On the other hand, when the thin film ($<100 \text{ nm}$) attached on a PDMS substrate is subjected to strain, multiple smaller cracks, instead of a single complete fracture, were usually observed due to strain delocalization by the polymer substrate (Fig. 1b). For instance, a pseudo-freestanding 40 nm P1 and 100- μm -thick P1 films completely ruptured at 6% and 16% strain, respectively (Supplementary Fig. 8). In contrast, a P1 film laminated onto PDMS (P1–PDMS) formed micro-sized cracks at 40% strain instead of suffering complete rupture (Supplementary Fig. 8). Based on this observation and previous theoretical studies²⁰, we hypothesize that if a polymer thin film is strongly bonded to an energy-dissipating layer, its strain may be more efficiently delocalized without delamination, and hence, crack initiation and propagation can be notably suppressed or delayed (Supplementary Fig. 9).

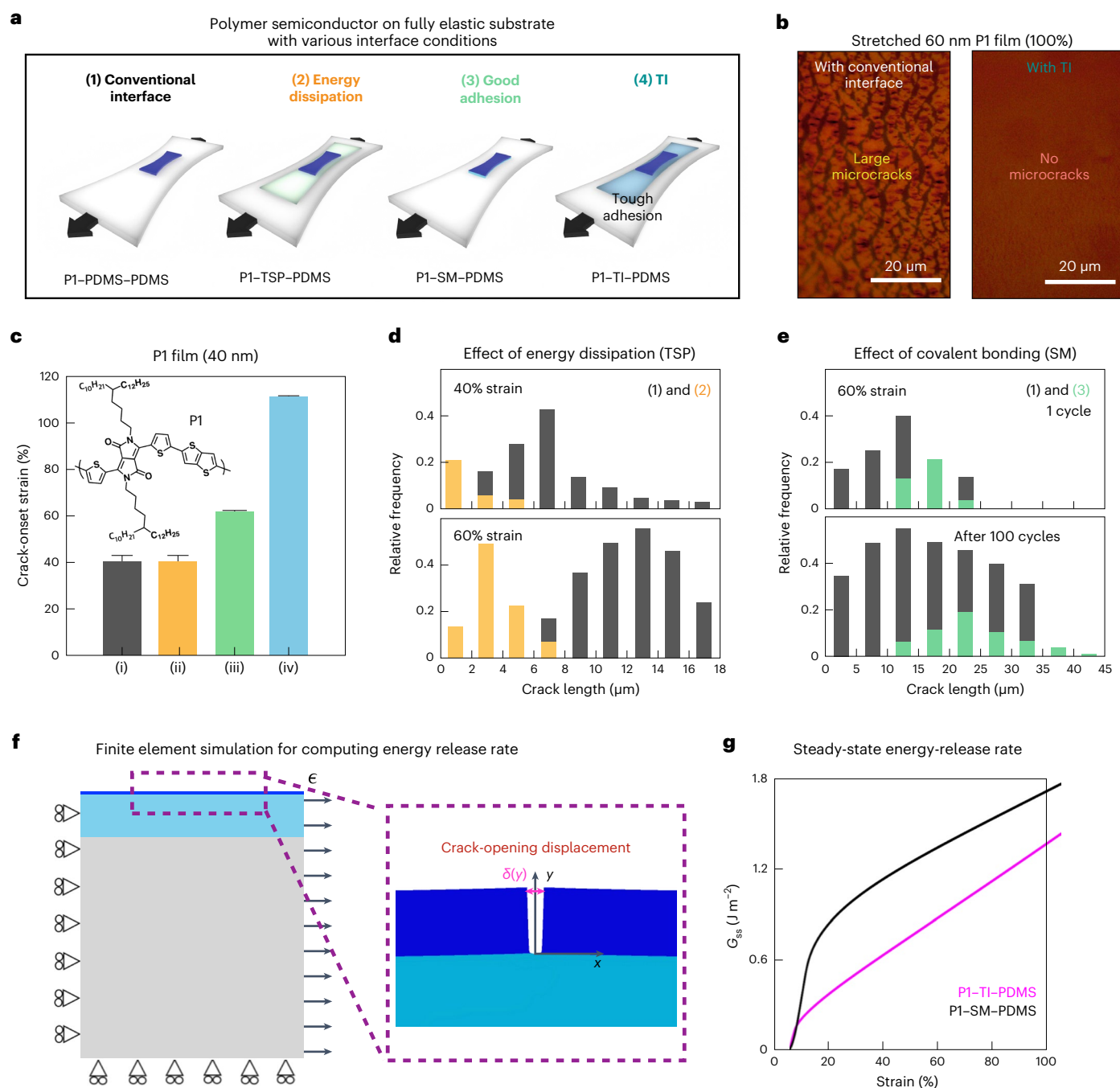


Fig. 3 | Delayed crack formation in semiconducting thin films by embedding a TI. **a**, Schematic of semiconducting thin films on an elastic PDMS substrate with various interface conditions. **b**, Optical microscopy images of (1) (left) and (4) (right) at 100% strain. **c**, Summary of crack-onset strains of P1 films with the different interface conditions shown in **a**; the error bars represent the results from three batches of samples. **d**, Histograms of the crack lengths in P1 films with condition (1) (black) and (2) (orange) under 40% (top) and 60% (bottom) strains. Data were collected from five images for each condition. We confirmed the effect of the energy dissipation of TI on delaying crack initiation and propagation.

e, Histograms of the crack lengths in P1 films with condition (1) (black) and (3) (green) under 60% strain (top) and after 100 stretching cycles under 60% strain (bottom). Data were collected from five images for each condition. We confirmed the effect of covalent bonding on delaying crack initiation and propagation. **f**, Finite element simulations to compute the energy-release rate for a steady-state channel crack of P1 in P1-TI-PDMS and P1-SM-PDMS multilayer structures, with the zoomed-in view showing the simulation result and definition of crack-opening displacement $\delta(y)$. **g**, Calculated steady-state energy-release rate G_{ss} (J m⁻²) as a function of strain (%) for P1-TI-PDMS and P1-SM-PDMS.

To validate our hypothesis, we first measured the crack-onset strain of P1 films with and without a TI layer on PDMS (P1-TI-PDMS and P1-PDMS-PDMS, TI = SM/TSP/SM) by optical microscopy. As shown in Fig. 3c, we observed a notably delayed crack-onset strain of P1-TI-PDMS from 40% to 110%, which is also accompanied by a continuous increase in the dichroic ratios via polarized ultraviolet–visible

(UV–vis) spectroscopy (Supplementary Fig. 10). In addition, we could not observe the strain-rate dependence on the crack-onset strain of P1-TI-PDMS. Even at a high strain rate of 1,000 min⁻¹, the crack-onset strain is notably delayed in P1-TI-PDMS (Supplementary Fig. 11).

To further understand the roles of TI, we first investigated the importance of energy dissipation in reducing crack initiation and

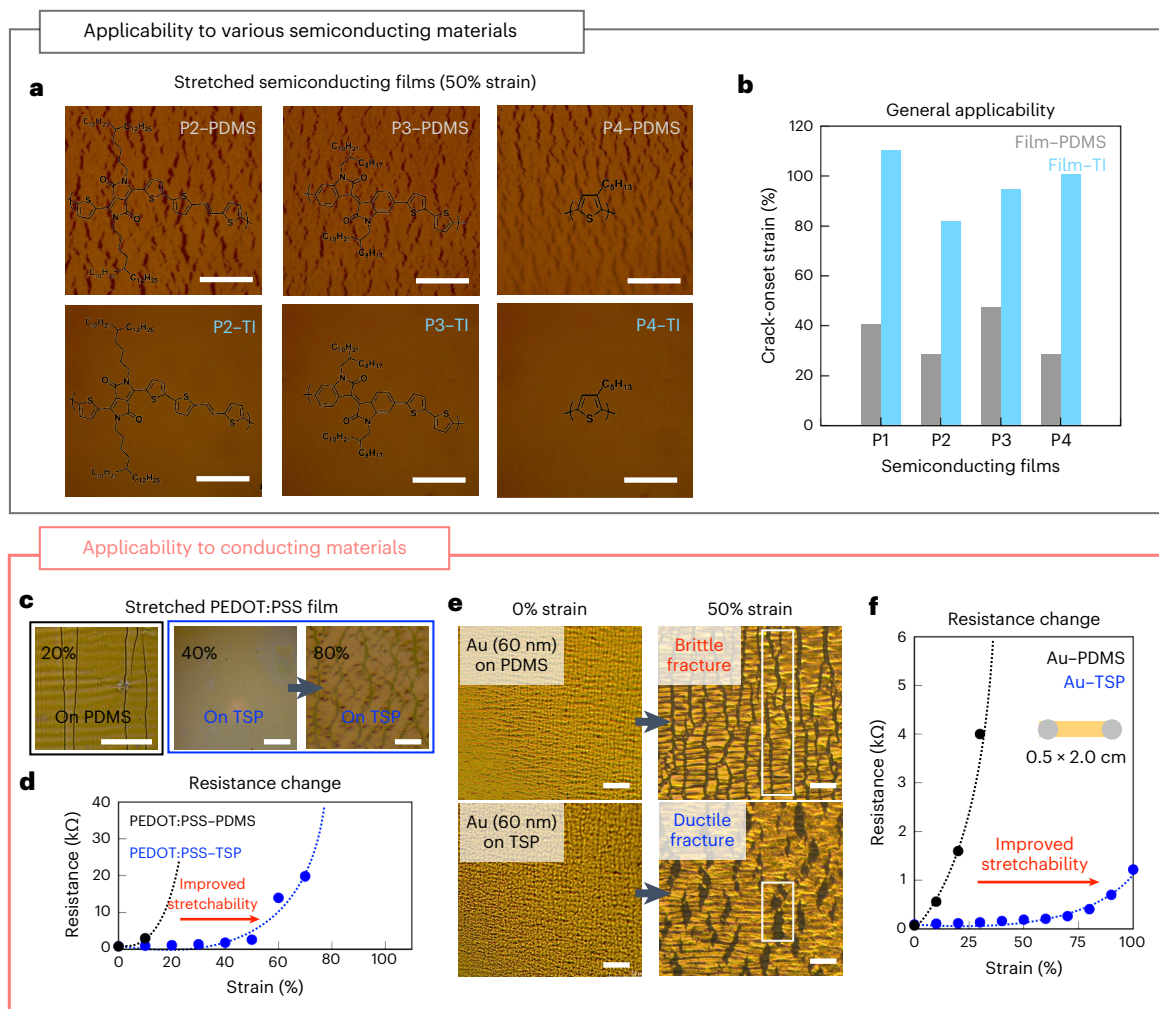


Fig. 4 | Broad applicability of TI to various polymer semiconductors and conductors. a, Optical microscopy images of Px-PDMS (top) and Px-TI (bottom) ($x = 2, 3, 4$) at 50% strain. Scale bars, 20 μm . **b,** Summary of crack-onset strains of Px films ($x = 1, 2, 3, 4$) with respect to various interface conditions. **c,** Optical microscopy images of stretched PEDOT:PSS films; PEDOT:PSS on PDMS at 20% strain (left) and PEDOT:PSS on TI at 40% (middle) and 80% (right) strain. The PEDOT:PSS film was directly spin coated on oxygen-plasma-treated PDMS and

TSP. Scale bars, 20 μm . **d,** Electrical resistance changes in the PEDOT:PSS film during stretching. The width, length and thickness of the sample are 0.5 cm, 2.0 cm and 50 nm, respectively. **e,** Optical microscopy images of Au films on PDMS (top) and TSP (bottom) at 0% strain (left) and 50% strain (right). Scale bars, 10 μm . **f,** Electrical resistance changes in Au films during stretching. The width, length and thickness of the sample are 0.5 cm, 2.0 cm and 60 nm, respectively.

slowing down crack propagation. Indeed, we observed substantially smaller crack sizes (7.0 to 1.5 μm) and crack numbers in P1-TSP-PDMS (P1 laminated on TSP-PDMS) compared with those in P1-PDMS-PDMS (P1 laminated on covalently crosslinked PDMS) (Fig. 3a,b,d and Supplementary Fig. 12). In addition, the cracks in P1-TSP-PDMS showed slower propagation on an additional applied strain. Next, the relative degree of crystallinity analysis was used to examine the morphological changes in P1 films under strain. The relative degree of crystallinity of P1-PDMS decreased more than that of P1-TSP-PDMS (80% versus 30%) as the tensile strain increased from 0% to 100% (Supplementary Figs. 13 and 14 and Supplementary Table 1). We also observed that the measured maximum dichroic ratio for P1-TSP-PDMS is 1.3 times higher than that for P1-PDMS (Supplementary Fig. 10). These results indicate that TSP enhances the bonding between layers and delocalizes strain in the P1 film, preventing crack propagation and breakage of crystalline domains. As a result, high strain induced more alignment of the polymer chains. The mechanism of energy dissipation through dynamic bond breakages within the semiconducting thin film has been previously observed to improve its intrinsic stretchability¹⁵, as well as increase interface adhesion²⁶. Here we confirm that

the energy-dissipating interface layer can be used to enable improved bonding and delay crack initiation and propagation in brittle polymer thin films.

Next, the effect of covalent bonding given by SM treatment was investigated. We observed delayed crack-onset strain for P1-SM-PDMS from 40% to 60% strain (Fig. 3c). Notably, at the crack-onset strain, P1-SM-PDMS showed lower crack density compared with that for P1-PDMS, indicating that the improved adhesion delayed crack initiation and propagation. This effect is more noticeable after 100 stress-strain cycles with 50% strain. As shown in Fig. 3e, P1-PDMS exhibits a substantial increase in crack sizes and density compared with P1-SM-PDMS (Fig. 3e and Supplementary Fig. 15). To exclude the possibility of microstructural changes in P1 caused by SM treatment, UV-vis spectroscopy and grazing incidence X-ray diffraction measurements were performed, which confirmed no observable changes in P1 aggregation behaviour and microstructures (Supplementary Fig. 16).

Next, we investigate the effect of the thickness of a polymer semiconducting film on its crack initiation and propagation in the presence of a TI. As films get thicker, they are expected to behave more like the bulk materials. As shown in Supplementary Fig. 17, even for a 100 nm

P1 film, the effect of TI on fracture behaviours is still present. The crack sizes in P1 (~125 nm)–TI–PDMS were five times smaller than those in P1 (~125 nm)–PDMS at the crack-onset strain (Supplementary Fig. 17).

We further observed that TI-stabilized stress–strain cycles as well as thermal cycles. Specifically, due to the plastic nature of P1 semiconducting films, wrinkle formation without delamination was observed for P1–TI after released from 100% strain (Supplementary Fig. 18). Wrinkle structures have been used as a strategy to achieve macroscopic reversible stretchability and provide an additional mechanism for stable stretching cycles for P1–TI films. In addition, we observed an improved thermal stability of P1–TI with no change in the crack-onset strain after thermal annealing at 100 °C for 10 min and no noticeable cracks even at 100% strain whereas P1–PDMS crack-onset strain reduced to 20% (Supplementary Fig. 19).

To better explain the mechanisms for TI design, we theoretically investigated the toughening mechanism of P1–TI–PDMS. Since it has been well established that energy dissipation in a hydrogel and its covalent bonding to another material are important in enhancing interfacial toughness^{25,26}, we assume that the bonding between layers in P1–TI–PDMS is strong enough so that no delamination occurs. This way, we focus on investigating the effect of the substrate and TI layer in delaying crack propagation. P1 is modelled as a power-law material (Methods and Supplementary Fig. 20), which can be predicted to form necking at 3% strain when freestanding and subsequently rupture with a single crack. However, when stretching P1–TI–PDMS, necking localization was observed to be prevented. We conducted two-dimensional (2D) finite element simulations to compute the energy-release rates of a multilayer structure of P1–TI–PDMS subjected to external strain (Methods, Fig. 3f,g and Supplementary Fig. 21). As a comparison, the energy-release rates for P1–SM–PDMS were also computed under the assumption of no delamination to estimate an upper bound of the critical strain for crack propagation, whereas delamination can produce a lower critical strain. Both TI and PDMS are modelled as Arruda–Boyce materials²⁴. The steady-state energy release rate G_{ss} as a function of strain ε is computed (Methods and Fig. 3f). Considering typical fracture energy Γ of polymer semiconducting thin films is of the order of 10 J m^{-2} (ref. 32), our simulations predict that a semiconducting thin film bonded perfectly to a substrate can survive a strain ε_c above 100% by using the condition $G_{ss}(\varepsilon_c) = \Gamma$ (Fig. 3g). This indicates that a semiconducting thin film firmly bonded to a substrate can be stretchable. Moreover, the energy release rate G_{ss} of P1–TI–PDMS is always lower than that of P1–SM–PDMS due to the higher stiffness of TI than PDMS, indicating that the addition of the TI layer can delay crack propagation by not only strengthening the interfacial adhesion but also reducing the crack opening by more strongly constraining the deformation of P1.

Finally, to study the electrical performance of the stretchable P1 film enabled by TI design, we proceed to fabricate a fully stretchable transistor in a bottom-gate–top-contact structure, with spray-coated carbon nanotube (CNT) networks as the electrodes, a $2.1 \mu\text{m}$ TI layer as the dielectric layer and a $100 \mu\text{m}$ PDMS (SYLGARD 184) film as the elastic substrate (Supplementary Fig. 22). The obtained devices exhibited standard field-effect transistor characteristics and average mobility of $0.73 (\pm 0.14) \text{ cm}^2 \text{ V}^{-1} \text{ s}^{-1}$ from nine devices (Supplementary Fig. 23). At 100% strain along the current flow direction, the calculated average mobility after correcting for changes in channel length and dielectric capacitance was still maintained at $-0.53 (\pm 0.16) \text{ cm}^2 \text{ V}^{-1} \text{ s}^{-1}$ even under 100% strain (Fig. 3c, Supplementary Fig. 24 and Supplementary Table 2). In addition, after 100 repeated stretching cycles at 0–50% strain, there was only a small change in the on current after the second stretch-and-release cycle, which was attributed to wrinkle formation in the P1–TI bilayer without delamination after the first stretch-and-release process (Fig. 4e and Supplementary Fig. 24). In comparison, when a $2\text{-}\mu\text{m}$ -thick covalently crosslinked PDMS, instead of the TI layer, was used as the dielectric layer, a notable drop in the on current was observed immediately after being stretched to 50% strain

(Supplementary Fig. 24). Furthermore, microcracks were observed in P1 on stretching.

The TI layer designed here is applicable to most semiconducting polymers. As an example, we applied it to three additional semiconducting polymers (Fig. 4a). All the thin films directly transferred on a stretchable covalently crosslinked PDMS substrate severely cracked when subjected to 50% strain. However, with a TI layer between the semiconducting films and the substrate again delayed crack initiation and propagation; therefore, we could not observe noticeable cracks even at 100% strain (Fig. 4a,b). TI can also be used to enhance the stretchability of other types of electronic material. For example, a conducting polymer (poly(3,4-ethylenedioxythiophene) polystyrene sulfonate (PEDOT:PSS)) thin film, which exhibits brittle fracture at 10% strain when deposited on a PDMS substrate³³, shows stable conductivity even under 100% strain with the TI layer (Fig. 4c,d and Supplementary Fig. 25). Similarly, TI can be introduced to a thin Au film (60 nm thick) on a PDMS substrate (Supplementary Fig. 26). The film was observed to change from a brittle to ductile fracture, resulting in a stretchable Au conductor (Fig. 4e,f)³³. Taken together, our work suggests that the TI approach may open new avenues for future developments in stretchable electronics by broadening material choices.

Online content

Any methods, additional references, Nature Research reporting summaries, source data, extended data, supplementary information, acknowledgements, peer review information; details of author contributions and competing interests; and statements of data and code availability are available at <https://doi.org/10.1038/s41565-022-01246-6>.

References

- Someya, T., Bao, Z. & Malliaras, G. G. The rise of plastic bioelectronics. *Nature* **540**, 379–385 (2016).
- Miyamoto, A. et al. Inflammation-free, gas-permeable, lightweight, stretchable on-skin electronics with nanomeshes. *Nat. Nanotechnol.* **12**, 907–913 (2017).
- Kang, J., Tok, J. B. H. & Bao, Z. Self-healing soft electronics. *Nat. Electron.* **2**, 144–150 (2019).
- Park, S. et al. Self-powered ultra-flexible electronics via nano-grating-patterned organic photovoltaics. *Nature* **561**, 516–521 (2018).
- Kaltenbrunner, M. et al. An ultra-lightweight design for imperceptible plastic electronics. *Nature* **499**, 458–463 (2013).
- Wagner, S. & Bauer, S. Materials for stretchable electronics. *MRS Bull.* **37**, 207–213 (2012).
- Chortos, A., Liu, J. & Bao, Z. Pursuing prosthetic electronic skin. *Nat. Mater.* **15**, 937–950 (2016).
- Lee, S. et al. Ultrasoft electronics to monitor dynamically pulsing cardiomyocytes. *Nat. Nanotechnol.* **14**, 156–160 (2018).
- Wang, S., Oh, J. Y., Xu, J., Tran, H. & Bao, Z. Skin-inspired electronics: an emerging paradigm. *Acc. Chem. Res.* **51**, 1033–1045 (2018).
- Wang, S. et al. Skin electronics from scalable fabrication of an intrinsically stretchable transistor array. *Nature* **555**, 83–88 (2018).
- Yang, J. C. et al. Electronic skin: recent progress and future prospects for skin-attachable devices for health monitoring, robotics, and prosthetics. *Adv. Mater.* **31**, 1904765 (2019).
- Kim, D.-H. et al. Stretchable and foldable silicon integrated circuits. *Science* **320**, 507–511 (2008).
- Kim, D.-H. et al. Epidermal electronics. *Science* **333**, 838–843 (2011).
- Root, S. E., Savagatrup, S., Printz, A. D., Rodriguez, D. & Lipomi, D. J. Mechanical properties of organic semiconductors for stretchable, highly flexible, and mechanically robust electronics. *Chem. Rev.* **117**, 6467–6499 (2017).

15. Oh, J. Y. et al. Intrinsically stretchable and healable semiconducting polymer for organic transistors. *Nature* **539**, 411–415 (2016).
 16. Mun, J. et al. Effect of nonconjugated spacers on mechanical properties of semiconducting polymers for stretchable transistors. *Adv. Funct. Mater.* **28**, 1804222 (2018).
 17. Zheng, Y. et al. An intrinsically stretchable high-performance polymer semiconductor with low crystallinity. *Adv. Funct. Mater.* **29**, 1905340 (2019).
 18. Zheng, Y., Zhang, S., Tok, J. B. H. & Bao, Z. Molecular design of stretchable polymer semiconductors: current progress and future directions. *J. Am. Chem. Soc.* **144**, 4699–4715 (2022).
 19. Xu, J. et al. Highly stretchable polymer semiconductor films through the nanoconfinement effect. *Science* **355**, 59–64 (2017).
 20. Suo, Z., Vlassak, J. & Wagner, S. Micromechanics of macroelectronics. *China Particuol.* **3**, 321–328 (2005).
 21. Xiang, Y., Li, T., Suo, Z. & Vlassak, J. J. High ductility of a metal film adherent on a polymer substrate. *Appl. Phys. Lett.* **87**, 161910 (2005).
 22. Lu, N., Wang, X., Suo, Z. & Vlassak, J. Metal films on polymer substrates stretched beyond 50%. *Appl. Phys. Lett.* **91**, 221909 (2007).
 23. Lee, S.-Y. et al. Selective crack suppression during deformation in metal films on polymer substrates using electron beam irradiation. *Nat. Commun.* **10**, 4454 (2019).
 24. Yang, J., Bai, R. & Suo, Z. Topological adhesion of wet materials. *Adv. Mater.* **30**, 1800671 (2018).
 25. Liu, Q., Nian, G., Yang, C., Qu, S. & Suo, Z. Bonding dissimilar polymer networks in various manufacturing processes. *Nat. Commun.* **9**, 846 (2018).
 26. Yuk, H., Zhang, T., Lin, S., Parada, G. A. & Zhao, X. Tough bonding of hydrogels to diverse non-porous surfaces. *Nat. Mater.* **15**, 190–196 (2016).
 27. Yuk, H., Zhang, T., Parada, G. A., Liu, X. & Zhao, X. Skin-inspired hydrogel–elastomer hybrids with robust interfaces and functional microstructures. *Nat. Commun.* **7**, 12028 (2016).
 28. Wang, G. N. et al. Tuning the cross-linker crystallinity of a stretchable polymer semiconductor. *Chem. Mater.* **31**, 6465–6475 (2019).
 29. Lee, H., Lee, B. P. & Messersmith, P. B. A reversible wet/dry adhesive inspired by mussels and geckos. *Nature* **448**, 338–341 (2007).
 30. Kang, J. et al. Tough and water-insensitive self-healing elastomer for robust electronic skin. *Adv. Mater.* **30**, 1706846 (2018).
 31. Sun, J. Y. et al. Inorganic islands on a highly stretchable polyimide substrate. *J. Mater. Res.* **24**, 3338–3342 (2009).
 32. Zhang, S. et al. Directly probing the fracture behavior of ultrathin polymeric films. *ACS Polym. Au* **1**, 16–29 (2021).
 33. Wang, Y. et al. A highly stretchable, transparent, and conductive polymer. *Sci. Adv.* **3**, e1602076 (2017).
- Publisher's note** Springer Nature remains neutral with regard to jurisdictional claims in published maps and institutional affiliations.
- Springer Nature or its licensor (e.g. a society or other partner) holds exclusive rights to this article under a publishing agreement with the author(s) or other rightsholder(s); author self-archiving of the accepted manuscript version of this article is solely governed by the terms of such publishing agreement and applicable law.
- © The Author(s), under exclusive licence to Springer Nature Limited 2022

Methods

Sample preparation

P1- $X-X'$ means that the P1 film is on the X' substrate with the X interface layer. For SM, we used SM-1 (perfluoroazide version) for most of the experiments. We also designed SM-2 (benzophenone version), which can readily crosslink with almost any surface with C-H bonds as another universal crosslinker.

Px-PDMS-PDMS: a polymer semiconductor film (Px, 40 nm) was prepared on octadecyltrichlorosilane (OTS)-treated SiO₂. A PDMS layer (2 μ m) was directly spin coated on Px from a PDMS solution (5 g SYLGARD 184 precursor:crosslinker = 15:1 in 20 ml hexane) at 2,000 rpm for 2 min. After annealing at 150 °C for 1 h, the resulting film was transferred onto another crosslinked PDMS substrate (precursor:crosslinker = 20:1; thickness, 200 μ m).

Px-SM-PDMS: a polymer semiconductor film (Px, 40 nm) was prepared on OTS-treated SiO₂. The SM solution in hexane (5 wt%) was first spin coated at 3,000 rpm for 1 min onto the polymer film and annealed at 150 °C for 1 h. The resulting film was transferred onto crosslinked PDMS substrates (precursor:crosslinker = 20:1; thickness, 200 μ m).

Px-TI-PDMS: a polymer semiconductor film (Px, 40 nm) was prepared on OTS-treated SiO₂. The SM solution in hexane (5 wt%) was first spin coated at 3,000 rpm for 1 min onto the polymer film and annealed at 150 °C for 1 h. Subsequently, SHP/SM (90/10, wt/wt ratio) solution (100 mg ml⁻¹) in hexane/IPA (95/5, v/v) was directly spin coated onto the polymer film-SM and annealed again at 150 °C for 1 h. The resulting film was transferred onto crosslinked PDMS substrates (precursor:crosslinker = 20:1; thickness, 200 μ m).

Fully stretchable transistor fabrication

For gate electrodes, CNT (P2-SWNT, Carbon Solutions) and poly(3-hexylthiophene-2,5-diyl) (P3HT) were dispersed in chloroform (0.20 mg ml⁻¹ CNT and 0.05 mg ml⁻¹ P3HT). Ultrasonication of the CNT/P3HT/chloroform mixture was conducted for 30 min at 30% amplitude using a 750 W ultrasonication probe. Centrifugation of the ultrasonicated solution at 8,000 rpm for 30 min resulted in a well-dispersed CNT solution in chloroform. The CNT supernatant solution was spray coated onto an OTS-treated SiO₂ wafer using a commercially available airbrush (Master Airbrush, SB844). The spray-coated CNT layer (~40 nm) was embedded into SHP (PDMS-MPU (4,4'-methylenebis(phenyl urea))_{0.3}-IU (isophorone bisurea)_{0.7}) (2 μ m thickness) and subsequently transferred onto a PDMS substrate (precursor:crosslinker = 15:1; thickness, 150 μ m). A semiconducting polymer solution was spin coated on an OTS-treated SiO₂ wafer at 1,500 rpm for 1 min. The thin film (40 nm) was annealed at 150 °C for 30 min. SM (5 wt% in hexane) was directly spin coated onto the annealed polymer thin films at 2,000 rpm for 1 min and subsequently annealed at 150 °C for 1 h. Next, the dielectric layer (that is, TI layer) was prepared by directly spin coating a TSP solution (80 mg ml⁻¹; SHP:SM = 9:1 wt/wt in hexane/IPA = 10/1 v/v) onto the annealed polymer semiconductor thin film. The thickness of the dielectric layer was around 2.1 μ m. The semiconductor-TI film on OTS-treated SiO₂ was further annealed at 80 °C overnight. Next, it was directly transferred onto the gate/substrate. For source/drain electrodes, CNT (P3-SWNT, Carbon Solutions) was dispersed in IPA. First, 0.3 mg ml⁻¹ CNT/IPA solution was bath sonicated for 4 h. Then, the solution was ultrasonicated for 30 min at 30% amplitude using a 750 W ultrasonication probe. The as-dispersed CNT solution was centrifuged at 6,000 rpm for 30 min. Finally, the well-dispersed CNT supernatant was directly spray coated onto the semiconductor layer using a commercial airbrush (Master Airbrush, SB844) and patterned through a metal shadow mask with a channel length of 150 μ m and channel width of 1,000 μ m.

Film characterization

The crack-onset strain was measured using 'film-on-elastomer' methods for various thin films. The crack onset was determined with an

optical microscope. In our experiments, we measured the actual applied strain to the semiconducting film and used it to determine the crack-onset strain of the film to avoid the different strain distribution problems caused by the interface layer. Thin-film UV-vis spectroscopy was performed with an Agilent Cary 6000i UV-vis-near-infrared spectrophotometer. Grazing incidence X-ray diffraction experiments were conducted at beamline 11-3 of the Stanford Synchrotron Radiation Lightsource. Electrical characterizations of the transistors and conductivity were carried out with a Keithley 4200 parameter analyser.

Finite element simulations

We calculated the steady-state energy release rate of the channel crack in a P1 film in P1-TI-PDMS and P1-SM-PDMS via finite element analysis using the ABAQUS finite element package. We first built 2D simulation models for P1-TI-PDMS and P1-SM-PDMS multilayer structures with a channel pre-crack in the P1 film, assuming no delamination between all the layers (Fig. 3f). We also built three-dimensional simulation models, but the energy release rate for steady-state crack propagation was similar to that of the 2D model; therefore, we only present the results from 2D simulations here. The geometric dimensions and symmetric boundary conditions of P1-TI-PDMS are shown in Supplementary Fig. 18a. For P1-SM-PDMS, the TI layer is simply omitted. The P1 film is modelled as a power-law material as

$$\varepsilon = \frac{\sigma}{E} \left(1 + \alpha \left(\frac{\sigma}{\sigma_y} \right)^{n-1} \right), \quad (1)$$

with the material law implemented in ABAQUS by fitting the experimental stress-strain curve to the Marlow free energy. In equation (1), ε is the strain, σ is the stress, Young's modulus E is fitted to the experimental measurement and is 600 MPa, the yield strength is fitted to be $\sigma_y = 6$ MPa, the yield offset $\alpha = 0.001$ and hardening exponent $n = 20$. Both TI and PDMS are modelled as Arruda-Boyce materials, with shear modulus $\mu = 2.400$ MPa and 0.150 MPa, respectively, and stretch limit $\lambda_m = 9.0$ and 2.4, respectively. We deformed the multilayer structures to external strain ε using displacement control, and computed the remote stress distribution $\sigma(y)$ across the film thickness and crack-opening displacement distribution $\delta(y)$ (Fig. 3f). Then, we can use the following formula to calculate the steady-state energy release rate G_{ss} as a function of ε :

$$G_{ss} = \frac{1}{2h} \int_0^h \sigma(y) \delta(y) dy, \quad (2)$$

where h is the film thickness^{34,35}. By comparing the steady-state energy release rate G_{ss} with the fracture energy of P1, that is, Γ , $G_{ss}(\varepsilon_c) = \Gamma$, we can determine the critical strain for steady-state crack propagation ε_c .

Shear-lag model

Using a shear-lag model, we can estimate the maximal strain in P1, namely, ε_{max} , when strain ε_{app} is applied to the PDMS substrate in P1-TI-PDMS as³²

$$\frac{\varepsilon_{max}}{\varepsilon_{app}} = 1 - \frac{1}{\cosh\left(\frac{L}{2\Lambda}\right)}, \quad (3)$$

where

$$\Lambda = \sqrt{\frac{E_{P1} h_{P1} h_{TI}}{\mu_{TI}}}, \quad (4)$$

E_{P1} and h_{P1} are Young's modulus and thickness of P1, respectively; μ_{TI} and h_{TI} are the shear modulus and thickness of TI, respectively; and L is the length of the multilayer structure. Given that $E_{P1} = 600.0$ MPa, $h_{P1} = 50$ nm, $\mu_{TI} = 2.4$ MPa, $h_{TI} = 2$ μ m and $L = 1.5$ cm, we can estimate $\Lambda = 5$ μ m and ε_{max} is almost equal to ε_{app} .

Data availability

The main data supporting the findings of this study are available within the Article and its Supplementary Information. Source data are provided with this paper.

References

34. Ambrico, J. M. & Begley, M. R. The role of initial flaw size, elastic compliance and plasticity in channel cracking of thin films. *Thin Solid Films* **419**, 144–153 (2002).
35. Beuth, J. L. & Klingbeil, N. W. Cracking of thin films bonded to elastic plastic substrates. *J. Mech. Phys. Solids* **44**, 1411–1428 (1996).

Acknowledgements

This work is supported by Samsung Electronics. J.K. acknowledges support from the National Research Foundation of Korea through grant nos. 2021R1C1C1011116 and 2021M3H4A1A03048658. J.M. acknowledges financial support from Samsung Scholarship. L.J. acknowledges support from the National Science Foundation through grant no. CMMI-1925790. We acknowledge J. Hutchinson of Harvard University for the insightful discussions. Part of this work was performed at the Stanford Nano Shared Facilities (SNSF).

Author contributions

J.K., J.M. and Z.B. conceived the concept and designed the experiments. J.K. synthesized and characterized the molecules and

polymers. Y.Z. provided the conjugated polymers. J.K., J.M., N.M., Y.Z. and G.H.L. designed the device experiments and evaluated the stretchability of materials and devices. J.K. and J.M. fabricated the fully stretchable organic thin-film transistors. M.K. and L.J. performed the mechanical simulations. J.M. and H.-C.W. performed the grazing incidence X-ray diffraction experiments and analysis. S.C. performed the X-ray photoelectron spectroscopy measurements. J.K., J.M., M.K., J.B.-H.T., L.J. and Z.B. wrote the paper.

Competing interests

The authors declare no competing interests.

Additional information

Supplementary information The online version contains supplementary material available at <https://doi.org/10.1038/s41565-022-01246-6>.

Correspondence and requests for materials should be addressed to Lihua Jin or Zhenan Bao.

Peer review information *Nature Nanotechnology* thanks Xiaodong Chen and the other, anonymous, reviewer(s) for their contribution to the peer review of this work.

Reprints and permissions information is available at www.nature.com/reprints.